POSTPRINT del artículo publicado en: Science of the Total Environment 536: 268-278 (2015)

Thallium occurrence and partitioning in soils and sediments affected by mining activities in Madrid province (Spain)

Gomez-Gonzalez[a], M.A., Garcia-Guinea[a], J., Laborda[b], F., Garrido[a*], F.

[a]National Museum of Natural Sciences, CSIC, Jose Gutierrez Abascal 2, 28006 Madrid, Spain

[b]Group of Analytical Spectroscopy and Sensors Group, Institute of Environmental Sciences, University of Zaragoza, Pedro Cerbuna 12, 50009 Zaragoza, Spain.

*Corresponding author: fernando.garrido@mncn.csic.es. T. +34 91 7452500

Keywords. Thallium, Cathodoluminescence, Soil contamination, Ag-Cu ores

ABSTRACT

Thallium (Tl) and its compounds are toxic to biota even at low concentrations but little is known about Tl concentration and speciation in soils. An understanding of the source, mobility, and dispersion of Tl is necessary to evaluate the environmental impact of Tl pollution cases. In this paper, we examine the Tl source and dispersion in two areas affected by abandoned mine facilities whose residues remain dumped on-site affecting to soils and sediments of natural water courses near Madrid city (Spain). Total Tl contents and partitioning in soil solid phases as determined by means of a sequential extraction procedure were also examined in soils along the riverbeds of an ephemeral and a permanent streams collecting water runoff and drainage from the mines wastes. Lastly, electronic microscopy and cathodoluminescence probe are used as a suitable technique for Tl elemental detection on thallium-bearing phases. Tl was found mainly bound to quartz and alumino-phyllosilicates in both rocks and examined soils. Besides, Tl was also frequently found associated to organic particles and diatom frustules in all samples from both mine scenarios. These biogenic silicates may regulate the transfer of Tl into the soil-water system.

1. INTRODUCTION

Thallium (Tl) and its compounds are highly toxic to animals, plants, and microorganisms (Jakubowska et al., 2007). In humans, Tl is absorbed through the skin and mucous membranes, it is widely distributed throughout the body and accumulates in bones, renal medulla and, eventually, in the central nervous system. Also, Tl passes through the placenta, occurs in milk, and is excreted mainly in urine. The biological half-life of Tl in man is 3-8 days (Zitko, 1975). In spite of it, there has been relatively little research on the chronic toxicity of Tl and the tissue levels of Tl, resulting from a chronic exposure and little is known about Tl concentration and speciation in soils. An understanding of the source, mobility, dispersion, and exposure to humans of Tl is necessary to evaluate the environmental impact of Tl pollution cases and implement appropriate remediation strategies (Xiao et al., 2012) as the conventional removal of heavy metals from wastewater has little effect on Tl (Peter and Viraraghavan, 2005).

Several studies on Tl incidence in French, Austrian and Chinese soils have shown a range of Tl concentration between 0.08 and 1.5 mg kg^{-1} in non-polluted soils (Tremel et al., 1997). However, in highly polluted soils affected by mine activities, Tl concentration may reach up to 70 mg kg^{-1} (Lis et al., 2003). More recently, the ecotoxicological importance of Tl emissions to the atmosphere after coal use for energy production has also been pointed out (Lopez Anton et al., 2013) and translocation and mobility of Tl from Zn-Pb ores to surrounding soils has been assessed by Karbowska et al. (2014) showing that the majority of Tl was found probably bound to sulfides (oxidizable fraction).

In geochemical systems, Tl(I) is dominant and as such, it substitutes for K(I) or Rb(I) in silicates (Gomez-Gonzalez et al., 2015). In hydrothermal systems, Tl is frequently associated to sulfide phases such as pyrite whose weathering releases Tl to the media including sedimentary rocks, Fe and Mn hydroxides, organic matter and coals (Lis et al., 2003). Thallium(III) is reported to be the most abundant species in sea and lake waters (Scheckel et al., 2004). Biological-driven oxidation of Tl(I) to Tl(III) has been described in freshwater due to the formation of stable complexes with inorganic and organic ligands (Scheckel et al., 2004). Recently, Peacock and Moon (2012) demonstrated the molecular-scale mechanism of Tl sorption to Mn oxides and marine ferromanganese precipitates through outer-sphere surface complexes in the case of Tl(I) uptake by ferrihydrite, triclinic birnessite and todorokite, or inner-sphere surface complexes for Tl(I) uptake by hexagonal birnessite previous oxidation to Tl(III).

Overall, Tl is often undetected and has been studied to a lesser extent than other toxic elements in soils and sediments even though it is highly toxic and usually discarded as part of the tailings in the environment. Moreover, naturally occurring Tl in soils and water has been considered a hidden geoenvironmental health hazard (Xiao et al., 2004) and the combined use of X-ray energy-dispersive spectrometer (EDS) and cathodoluminescence (CL) probes in the environmental scanning electron (ESEM) microscope allow for thallium elemental detection on thallium-bearing rocks (Gomez-Gonzalez et al., 2015). Also, a crucial factor of the potential toxic effect of Tl in the investigated soils is Tl mobility and this can be determined by a sequential extraction of soil (Lis et al., 2003).

A systematic research of Tl occurrence in soils and stream sediments nearby sulfide ore mining and smelting areas is thus important specially if they are close to water reservoirs or urban centers. To the best of our knowledge, there is no information on Tl

occurrence and solid-phase partitioning in mine-affected polluted areas of Madrid (Spain) province. Our objective is to investigate the Tl content in two mine-affected catchments and its speciation in the solid phase of soils and river sediments identifying the main mineral scavengers as well as to study Tl dispersion processes from the hosting minerals to the soils.

2. MATERIALS AND METHODS

2.1. Sites description

2.1.1. Site 1 (S1). El Verdugal area

The experiment was conducted in a shrubland situated in the upper portion of a small sub-catchment of the Guadalix River (Madrid, Spain), which feeds into the Madrid Tertiary Detrital Aquifer (Fig. 1a). From a geological point of view, the Verdugal mining area belongs to a granite pegmatite field hosted in the sillimanite-migmatite-gneis bodies. These pegmatites are complex exhibiting (1) border zones with tourmaline, (2) wall zones of quartz and perthite feldspars, (3) intermediate zones with apatite triplite and beryl, and (4) cores with rose quartz. These pegmatite structures were probably formed at circa 700-600ºC by fractional crystallization of granite melts enriched in volatile elements. In the Verdugal area case, this progressive process produced hydrothermal veins of mineralized quartz (W-Sn-As), epithermal deposition (Ag-Bi-Cu-Zn-F-Pb) and a final metasomatic fluid filling the pegmatite rock with Fe, Mn, Ba and Tl giving a final color brown to the samples rock.

In this area, arsenopyrite [FeAsS] encapsulated in quartz was mined and processed for wolfram extraction during the Second World War (Fig. 1c) (Recio-Vazquez et al., 2011). The site includes an abandoned smelting factory and the mining wastes, rich in scorodite [$FeAsO_4 \cdot 2H_2O$], contain up to 190 $g \cdot Kg^{-1}$ of As (Gomez-Gonzalez et al., 2014; Helmhart et al., 2012) and currently remain where they were dumped on the soil surface, thus subjected to erosion and weathering processes. Bovine cattle have long been raised in a farm adjacent to the area in which high As concentrations has been determined in previous studies (Gomez-Gonzalez et al., 2014).

2.1.2. Site 2 (S2). Mónica Mine

Site 2 is located along the La Mina stream gorge (Bustarviejo village, NW Madrid, Spain) that collects water drainage from an abandoned mine. From a geological point of view, the As-Ag-bearing mineralized veins of quartz are hosted in gneisses displaying a

characteristic high-temperature assemblage of biotite, sillimanite, and garnet, together with quartz, K-feldspar and plagioclase. The veins are characterized by multistage ore deposition belonging to four mineralizing stages, as follows: (I) (As-Fe) with arsenopyrite, pyrite, quartz and muscovite, (II) (Zn-Cu-Sn) with sphalerite, chalcopyrite, pyrrhotite and pyrite, (III) (Pb-Ag) Galena, Ag-Bi sulphosalts, native bismuth, quartz and (IV) supergenic alteration with marcasite, covelline, scorodite and goethite (Martin-Crespo et al., 2004). The As-(Ag) sulphide vein system of Mónica mine was exploited from the seventeenth to the twentieth century (closed in 1980), mainly for Ag and Cu extraction (Fig. 1b). The pyritic residues remain dumped outside and heavy metal contamination of the mine surroundings has been previously reported (Moreno-Jimenez et al., 2010; Moreno-Jimenez et al., 2009) although no reference to the presence of Tl has been done before. Monitoring metal pollution level in these soils is necessary as the area has been classified as a leisure site inside an environmental reservoir proposed for the ecological network Natura 2000, following the environmental directives of the European Union (Council-Directive).

2.2. Sampling and soils properties

From S1, 0-15 cm depth bulk samples were collected at: (1) the main waste pile (WP) dumped on the soil surface (S1-WP); (2) at 17 m downstream from the WP from the riverbed (RB) of a small ephemeral stream that collects runoff originating at the wastes; (S1-RB); (3) the sediment from a downstream pond (SP) at 58 m from the WP (S1-SP), and (4) a flat area of land at ~100 m from the WP, on an adjacent farm for cattle breading that receives the excess runoff that overflows the pond during intense rain events (S1-F). At the sampling time, there was no surface waterflow. Approximate distances between sampling points and a general overview of the area are shown in Fig. 1C. Similarly, from S2, 0-15 cm depth bulk samples were taken from: (1) the arsenic-bearing waste pile (S2-WP), and (2) three additional sampling points located at 135, 380, and 740 m from the mine residues along the La Mina gorge downstream (S2-A, S2-B, S2-C, respectively) and adjacent to the water course (Fig. 1B). Additional rock samples from the waste piles of S1 and S2 sites were taken for their observation and analysis by electron microscopy and cathodoluminescence.

All soil samples were taken to the laboratory, air-dried, homogenized, and sieved (2-mm mesh) prior to analysis. Texture was determined by the pipette method after removing soil organic matter (Gee and Bauder, 1986). Soil pH and electrical

conductivity were measured in deionized water (1:5 m/m suspension). Total organic carbon (TOC) was determined by wet digestion (Walkley and Black, 1934). Exchangeable bases were extracted with 1 M NH_4OAc (at pH 7) (Thomas, 1982), and exchangeable Al was extracted with 1 M KCl (Barnishel and Bertsch, 1982). The Ca, Mg, Na, K, and Al concentrations in the extracted solutions were determined by inductively coupled plasma-optical emission spectrometry (ICP-OES) on a Perkin-Elmer OPTIMA 4300DV. In addition, all samples were dissolved by the application of two sequential digestion steps, followed by a microwave assisted digestion at 200ºC during 15 min (Ethos Series 1, *Milestone*): Step I – $HF/HNO_3/HCl$ (volume ratio 1.5:0.75:3.5) and Step II – H_3BO_3 (5%). Solutions from the digestion process were filtered and analyzed for total As, Mn, Pb and Tl content by inductively coupled plasma-mass spectrometry (ICP-MS) on an ELAN DRC-e (*Perkin Elmer)* and for total Fe content by inductively coupled plasma-optical emission spectrometry (ICP-OES) on an Iris & Intrepid Radial (*Thermo Fisher Scientific*). A reference material (NIST SRM 2711) was employed to check the validity of the digestion method.

All the chemicals used for sample preservation, analysis and reagent preparation were of reagent grade quality or higher. Deionized water (18 MΩ-cm, Milli Q+, Millipore Corp) was used for all solutions and dilutions. For all elemental determinations performed by ICP-MS/OES, calibration curves were run before and after each sample series (20 samples including matrix-matched blanks and in-between calibration checks). The calibration solutions covered the range of concentration in the samples and were prepared in the same matrix as the extracting reagents from certified stock solutions. Sample blanks were analyzed for correction of background effect on instrument response. Trace metal standards were used to assess instrument precision. We calculated metal concentrations in unknown solutions on the basis of the external calibration averaging the concentrations from two repetitions for each experimental replication. Limits of detection were calculated as three standard deviation of the instrument response from 10 repeated analyses of sample matrix-matched blank solutions.

2.3. Sequential extraction procedure

A crucial factor of the potential toxic effect of Tl in the investigated soils is Tl mobility. This can be determined by a sequential extraction of soil (Lis et al., 2003). Samples were subjected to a three-step sequential chemical extraction scheme proposed by the Standards Measurement and Testing Programme (Rauret et al., 1999), modified by

Yang et al. (2005) (Table 1): (FI) fraction extracted with 0.11 M acetic acid corresponding to exchangeable and weak acid soluble fraction; (FII) fraction extracted with 0.1 M hydroxylamine hydrochloride at pH 2 targeting poorly crystalline or reducible Al, Fe and Mn (oxihydr)oxides; and (FIII) fraction extracted in 30% hydrogen peroxide and 1 M ammonium acetate targeting organic matter or oxidizable phases (sulfides). The residual fraction (R) was analyzed for total Tl concentrations after the FIII extraction using microwave-assisted digestion as described above. All determinations of Tl concentrations were done by inductively coupled plasma-mass spectrometry (ICP-MS).

The NIST SRM 2711 (Montana soil) certified reference material (CRM) from the National Institute of Standards and Technology (USA) was also subjected to the sequential extraction procedure in order to perform a quality assessment. This CRM is only certified for total Tl content, but can be useful for evaluating the Tl extractability. Results from Tl fractionation in SRM 2711 reference material can be found in Villar et al. (2001).

2.4. Environmental scanning electron microscopy (ESEM).

Polished sections of Tl-bearing rocks associated to hydrothermal metallic sulfides and all soil samples were analyzed in the Environmental Scanning Electron Microscope (ESEM XL30, FEI Company) with an X-ray energy-dispersive spectrometer (EDS) (Oxford Instruments) and coupled to a MONOCL3 Gatan probe to collect Tl cathodoluminescence (CL) spectra from the samples. The ESEM enables high-resolution observation, chemical analysis and spatially-resolved spectral cathodoluminescence of nonconductive specimens operating in low vacuum mode. For the Tl samples case we chose to avoid gold coverings facilitating the cathodoluminescence emission from the sample inside. The ESEM resolution at low vacuum was 3.0 nm at 30 kV (SE), 4.0 nm at 30 kV (BSE), and <12 nm at 3 kV (SE). The accelerating voltage was 200 V to 30 kV and the probe current up to 2 μA was continuously adjustable. In addition, this microscope has a coupled MONOCL3 probe to record CL spectra and panchromatic and monochromatic plots with a photomultiplier attached tube to the ESEM. The photomultiplier covers a spectral range of 185–850 nm and is more sensitive in the blue parts of the spectrum. A retractable parabolic diamond mirror and the photomultiplier tube were used to collect and amplify luminescence. The sample was positioned at 16.2 mm underneath the bottom of the CL mirror assembly.

The excitation for CL measurements was provided at 25-kV electron beam. Monochromatic CL plots at 560 nm allow for the identification of Tl in different minerals by (1) identifying Tl spots by monochromatic CL, (2) EDS analysis including Tl, and (3) recording CL spectra focused on selected spots to observe emissions at ~280 nm associated to oxygen vacancies produced by the intrinsic inert pair effect of Tl and peaks at ~560 nm attributed to the electronic dissociation of Tl molecules under the electron beam.

2.5. X-Ray Diffraction (DRX).

The semi-quantitative mineralogical composition of the total (≤ 2 mm) and clay (≤ 2 μm) fractions of the soil samples was determined by powder X-ray diffraction (XRD) with a Philips PW-1710/00 diffractometer using a CuKα radiation source with a Ni filter and a setting of 40 kV and 40 mA. Samples were carefully milled over a period of 15 min and pressed to produce pellets of powdered aliquots. The XRD data were processed using the XPOWDER software. XRD patterns were obtained by step scanning, from 3º to 65º 2θ, with a count for 0.5 s/step, an exploration speed of 7 º/min, and a 40 kV and 40 mA setting for the X-ray tube. The qualitative search-matching procedure was based on the ICDDPDF2 and the DIFDATA databases.

3. RESULTS

3.1. Sites characteristics

Both areas were characterized by the presence of mine residues with physical, chemical and mineralogical properties different than those shown in the downstream sampling points (Tables 2 and 3). In S1, the WP was acid, saline, poor in organic matter, and rich in scorodite and gypsum. Downstream, all samples increased their pH and organic matter while decreased their EC and showed a mineralogy dominated by illite, kaolinite and quartz. Likewise, in S2 area, the wastes differed clearly from the rest of samples. In this case, the wastes showed a sandy texture, high EC as well as low pH, ECEC, and organic matter content. The clay mineralogy was dominated by montmorillonite and jarosite. Soils sampled downstream were characterized by lower EC and larger ECEC, high organic matter content and a clay mineralogy dominated by phyllosilicates and quartz while jarosite was not detected (Tables 2 and 3).

3.2. Elemental composition

Total concentrations of As, Mn, Pb, Fe and Tl are given in Table 4. All the element concentrations were highest in both mine residues decreasing with distance from the source except for the Mn in site S2 with a concentration in the residues (148 mg kg^{-1}) one order of magnitude lower than those found downstream (averaging 1592 mg kg^{-1}). Although As concentration in the source of S1 site (S1-WP, 143 g kg^{-1}) was higher than in the S2-WP, As concentrations in S2 downstream samples were significantly higher than those in S1. For both S1 and S2 areas, total Tl concentrations were higher in the mine wastes than in the samples downstream but there is no tendency to decrease with the distance with respect to their mine sources. Thallium concentrations are at or above the reference concentration legally considered for non-contaminated soils in the area of the study (0.39 mg kg^{-1}; BOCM, 2007).

Montana soil (NIST SRM - 2711) was analyzed following the same procedure as described for the samples, resulting in similar concentrations values than the certified ones, especially in the Mn, Pb and Tl concentrations. These analyses validated the microwave digestion and ICP determination methods used for the environmental samples.

3.3. ESEM-EDS-CL observations and quantifications

3.3.1. Thallium-hosting rocks

Selected ESEM images of rocks and soil samples from S1 and S2 are presented in figures 2 to 5. The combined use of EDS and CL probes coupled to ESEM allow for Tl detection on thallium-bearing minerals of rocks and soil samples. The analytical routine, however, must circumvent some difficulties, as follows: (i) the spectral position of the main EDS line for both, S and Tl elements, is sited at circa 2.4 keV and the accessorial Tl EDS lines (at circa 1.8, 2.6, 8.9, 10.3, and 11 keV) are under the observation threshold. As a result, overlapping peaks obstruct a simultaneous detection of Tl and S and thus, Tl analyses in sulphide phases. Fortunately, late natural hydrothermal processes usually remobilize Tl from sulphide minerals to the surrounding host sulphur-free minerals, (ii) Tl inclusions in Fe sulphides are common (e.g., pyrite, chalcopyrite) and their hydrothermal or environmental alteration produces iron oxo-hydroxides which are luminescence killer solids. The potential detection of Tl areas onto such Fe minerals, via mono-chromatic CL plots, e.g., centered in the powerful green spectral peak of Tl, must be disregarded by a shortage of light emission.

Figure 2 shows EDS analyses and CL spectra of paragenetic minerals in a selected rock collected in the nucleus of a pegmatite body of El Verdugal area (Guadalix, Madrid – S1 site) within a red colored hydrothermal vein (Figures 2a and 2b) and accessible through an abandoned trench opened during the mine exploitation. This rock sample was formed in a late hydrothermal phase of the pegmatite body geological formation in which precipitated neo-formed adularia ($KAlSi_3O_8$), quartz (SiO_2), albite ($NaAlSi_3O_8$), muscovite ($KAl_2(Si_3Al)O_{10}(OH)_2$) and accessorial micro-crystals of monazite ($(Ce,La,Nd,Th)PO_4$), Mn-nodules rich in Pb, and baryte ($CaSO_4$), rutile (TiO_2) and thallous phases (Figures 2c and 2d). The presence of Tl at trace concentrations was commonly observed in most of phases through EDS analyses (Figure 2c). The spectral CL emissions were collected in the same spots (Figure 2d) to confirm the Tl existence. The characteristic CL spectral bands of Tl at ~280 nm associated to oxygen vacancies and ~560 nm attributed to the electronic dissociation of Tl molecules was found associated to Tl presence (Figure 2d).

Figure 3 displays EDS analyses (Fig. 3d), CL spectra (Fig. 3e), monochromatic (560 nm) (Fig. 3c) and backscattering ESEM plots (Fig. 3b) of a mineralized rock collected from the mine wastes in Mina Mónica (Bustaviejo, Madrid – S2 site). The representative rock exhibits large phenocrystals of K-feldspar metasomatized by hydrothermal fluids containing silica and iron oxides together with primary sulphide and sulphosalts such as arsenopyrite, pyrite, chalcopyrite, sphalerite, galena and lillianite and secondary covelline, scorodite and goethite (Figure 3a). The monochromatic plot of CL at 560 nm detaching the maxima CL emitting areas (Figure 3c) associated to the electronic dissociation of Tl molecular dimers helps identifying Tl-hosting minerals. The spectral CL let us to record CL patterns of the alkali feldspar areas showing luminescent K-feldspars by intrinsic defects and accessorial Tl; however albite phases exhibited richer areas in Tl and stronger Tl-associated luminescent features probably attributed to cluster micro-inclusions of thallous oxides (Figure 3e).

3.3.2. Thallium in soils

Primary Tl-hosting minerals described in the rocks were also found in soils from both S1 and S2 sites (Figures 4 and 5, respectively) with similar Tl content in their composition as determined by EDS. Albites, feldspars or quartzes were the main Tl-hosting mineral phases in both sampling sites in all cases showing the same cathodoluminescence (CL) emission features as above described. Besides, Tl was also

frequently found associated organic particles and diatom frustules in all samples from both mine scenarios and consequently, the Tl characteristic CL emission peak at 560 nm was also recorded.

3.5. Thallium sequential extraction

The results for the sequential extractions of the samples are presented in Table 5. In site S1, Tl was primarily extracted in step IV or residual fraction (ranging from 89 % in the samples from the WP to over 97 % in downstream S1-SP and S1-F samples) targeting alumino-silicates and other well crystallized minerals. The fraction of the total Tl concentration associated with step II which targets Fe and Mn (oxyhydr)oxides decreased from 6 % in the S1-WP sample to 3.6 % in the S1-RB and over 1 % in the S1-SP and S1-F samples. Thallium removed in step III targeting organic matter and other oxidizable fractions varied from approximately 3 % in S1-WP and S1-RB samples to 1 % the samples downstream.

Lastly, no Tl was extracted in the first extraction step (I) targeting the most extractable and exchangeable fraction of the total Tl content except in the S1-WP sample from which 1.6 % of total Tl was found associated to this extraction step.

In S2, Tl was also mainly removed in the last step of the sequential extraction scheme (step IV) targeting Tl bound to well crystallized minerals (Table 5). However, in contrast to S1 samples, in S2 the amount of Tl associated to this nominal fraction were greatest in S2-WP (approximately, 94 %) while in the samples downstream this fraction decreased to a mean value equal to 88 %. Thallium associated to Fe/Mn (oxyhydr)oxides (step II) was greater in S2 samples than in S1 ones reaching 5 % in the S2-WP sample and ranging from 4.9 % to 11 % in the downstream samples. The amount of Tl bound to the oxidizable fraction (step III) was low in the S2-WP sample (1 %) and increased with distance from the waste pile from 2.3 % in S2-A sample to 3.6 % in S2-C. Lastly, the amount of Tl released by step I varied from 0.1 % to 3.2 % in the samples downstream while virtually no Tl was associated to this fraction in the S2-WP sample.

Thallium fractionation in SRM 2711 reference material produced similar results to those showed by Villar et al. (2001).

4. DISCUSION

4.1. Geogenic Thallium in mine soils.

Thallium has been described in hydrothermal quartz veins of metallic ore deposits, generally associated to primary and secondary minerals (Tatsi and Turner, 2014; Vanek et al., 2015; Xiao et al., 2012). Thallium element is a guide for ore deposits of hydrothermal metals since their associated rocks are enriched in Rb, Tl and K elements (Ikramuddin et al., 1983; Massa and Ikramuddin, 1986; Shah et al., 1994).

Soils developed associated to zones of hydrothermal mineralization in mining areas are susceptible to contain high background of Tl concentration which when coupled with favorable hydrological regime, could potentially contaminate the environment. The similar nature of the main Tl-hosting minerals found in primary rocks and downstream soils in both S1 and S2 sites, as well as the low chemical extractability of Tl in soils, indicate that Tl spreading from mine wastes is related to the physical decomposition of mineralized rocks, natural erosion, and later pedogenic processes giving raised to Tl contents over natural backgrounds.

In both S1 and S2 sites, there is a gradient of Tl concentration from the residues to the soils and in the soils downstream indicating that there is a continue Tl dispersion process from the mineralized wastes area decreasing with distance from the source to background levels. Overall, our results indicate that Tl in the contaminated studied soils is related to mineralization natural geogenic Tl enhanced by the exposition of mine residues to atmospheric conditions.

4.2. Total Thallium concentration

The presence of mine residues in both S1 and S2 zones produces the release of toxic elements and their spreading along the ephemeral (S1) and permanent (S2) streams in concentrations over the established legal limits. However, the spatial distribution of As and Pb concentrations shows the pollution processes in scenario S2 to be more acute than in S1 (Table 4). Differences in the hydrological regime between both areas may explain the greater dispersion of toxic elements in S2. Ephemeral and seasonal water course in S1 area could limit the contamination downstream.

Compared to As and Pb concentrations, those determined of Tl are apparently low. However, Tl concentrations in our experimental sites are higher than the background and baseline Tl concentration levels (0.2 and 0.64 mg kg^{-1}, respectively) in soils from south-east Spain (Martinez-Sanchez et al., 2009). Moreover, total Tl concentrations determined in this study are within the range encountered in both acidic and neutral or slightly alkaline soils affected by pyrite tailings after the mining spill at Aznalcóllar

(Spain) in 1998 and considered moderately contaminated (1 - 5 mg kg^{-1}) (Martin et al., 2004). Likewise, Jakubowska et al. (2007) found ca. 0.4 mg kg^{-1} of Tl in soils from foodplain terraces near a Pb-Zn ore deposit area and Yang et al. (2005) also found 3 to 15 mg kg^{-1} of Tl in topsoils and ca. 2 mg kg^{-1} of Tl at more than 14 cm depth in soils affected by a pyrite slag pile. Stafilov et al. (2013) found up to 1.4 mg kg^{-1} of Tl in soils surrounding a former As-Sb mine. Lastly, Xiao et al. (2004) highlighted that Tl contents over 1 mg kg^{-1} in arable soils should be considered a geoenvironmental hazard due to Tl tendency to be absorbed by plants. As a result, in this context, total Tl concentrations found in scenarios S1 and S2 should be considered indicative of potential hazard for the soil-water system in the areas.

4.3. Thallium partitioning in soils

To provide reliable identification of the cause of pollution, it is important to ask what kinds of base-level data exist concerning the natural migration of toxic elements (Xiao et al., 2004). Significant information can be given by the element distribution in soil solid nominal fractions as determined by a sequential extraction procedure. Our results from the study of distribution of Tl in soil fractions indicate that most of primary Tl originating in the mine wastes has not been weathered and redistributed into more labile and extractable fractions. Thallium entrapped in the residual parent material (step IV of the fractionation procedure) is the major fraction in all samples from both S1 and S2 sites (Table 5). This Tl fraction can be ascribed to aluminosilicates and well crystallized minerals as the main reservoirs for the natural Tl in the soils which is in accordance with the results of the SEM observations and EDS analyses. In contrast, Tl bound to labile fractions (steps I, II, and III) sums up to 11% in the waste pile (WP) and decrease to 3 % in the farm soil downstream in the S1 site. These proportions are higher in S2 soils reaching 17 %. Within these fractions, that nominally bound to Fe and Mn (oxyhydr)oxides (step II) is the most important labile Tl fraction reaching approximately 50 % of the amount extracted in the first three steps in soils from S1 zone and a decreasing proportion from 80 % in the slag (S2-A) to 56 % in the furthest sampling point downstream in S2 zone (S2-F). However, at the pH of the soils (Table 2) and in contrast to other toxic elements, Tl does not significantly sorb to Fe oxides (Jacobson et al., 2005; Smeaton et al., 2012) although Martin et al. (2004) found that amorphous Fe and Al oxides were the main soil scavengers of Tl in acidic and neutral soils polluted by pyrite tailings. Instead, Mn oxides may have an important role

retaining Tl (Jacobson et al., 2005; Peacock and Moon, 2012; Tremel et al., 1997) although ESEM-EDS analyses do not show any close association of Tl to Mn mineral phases nor Tl and Mn total concentrations correlate. Only the greater Mn content in S2 than S1 sites may account for the greater proportion of Tl released upon the step II in the S2 samples as compared to that in S1 ones and be evidence of the tendency of Tl to be retained in Mn oxides as it is described in the literature (Vanek et al., 2013; Vanek et al., 2011). However, ESEM-EDS analyses have shown large amounts of pennate diatom frustules characterized with a typical bilateral symmetry in S1 and more frequently in S2 soil samples (Figures 4e and 5e). Biological surfaces of diatoms may contain functional groups with great capacity of reacting with both protons and metal ions (Gonzalez-Davila et al., 2000). The amphoteric nature and the affinity for metal adsorption of the siliceous skeleton are largely controlled by organic layers covering the frustules (Gelabert et al., 2004). As a result, they exert a strong control on the transfer of metals along the water column to soils and sediments, thereby regulating the concentration of dissolved metal ions in fresh water and diatoms being at the beginning of the trophic chains. In natural settings, bacteria degrade the organic membrane of diatoms after their death thus progressively exposing the underlying silica frustules to the aquatic environment. This is accompanied by a dramatic shift in metal binding properties and surface reactivity. For example, up to 90% of total trapped metals, located in the proton-binding sites of organic coatings (Pokrovsky et al., 2002) are likely to be released in the environment during diagenesis of diatom cells (Gelabert et al., 2006). However, when porous polysaccharidic layers decay, silanol groups of frustules may become exposed to freshwater leading to Tl retention. This fraction could also be extracted within the second step of the sequential extraction procedure.

Thallium associated to the oxidisable fraction (nominally, organic matter and sulfides) is less important in accordance to the weak tendency of Tl to bind to organic matter as compared to other monovalent metals (Jacobson et al., 2005), regardless the large OM content in S2 soils, and the oxidative conditions found in both experimental sites that reduces the stability of sulfide mineral phases. Lastly, the amount of Tl released in step I (exchangeable fraction) is negligible in all samples.

These results are in agreement with those of Yang et al. (2005) who found up to 98% of total Tl content associated to the residual fraction and help discriminating anthropogenic vs natural Tl in soils. In contrast, Vanek et al. (2011) found a majority of Tl bound to the reducible fraction (soil oxides) and a significant amount associated to the labile

fraction in artificially Tl contaminated soils. Based on this, spreading of Tl in both studied areas is related to the dissemination of non-weathered natural Tl-bearing quartz and aluminum-silicate large (i.e. non-colloidal size) particles with low transference to labile phases and biota. The continuous release of these particles to freshwater courses produces the accumulation of Tl in affected soils in spite of the limited mobility of Tl when it is bound to primary mineral particles. In addition, the role of Fe and Mn oxides as potential Tl scavengers cannot be deduced from our results. Instead, biogenic amorphous silicates could be significantly contributing to limit the incorporation of Tl into the soil-water system.

5. CONCLUSIONS

Soils developed in the vicinity of hydrothermal mineralization zones in mining areas are susceptible to contain high levels of Tl concentration. The exposition of mine wastes to atmospheric conditions and a favorable hydrological regime could potentially contaminate the environment. As a result, total Tl concentrations found in scenarios S1 and S2 should be considered indicative of potential hazard for the soil-water system in the areas.

Thallium spreading from mine wastes is related to the physical decomposition of mineralized rocks, natural erosion, and later pedogenic processes giving raise to Tl contents over natural backgrounds. Based on partitioning studies, spreading of Tl in both areas is related to the dissemination of non-weathered natural Tl-bearing quartz and aluminum-silicate large (i.e. non-colloidal size) particles with low transference to labile phases and biota. Besides, biogenic amorphous silicates could be significantly contributing to the Tl spreading and therefore may limit the incorporation of Tl into the soil-water system.

Full knowledge of the source, dispersion, and exposure to humans of Tl is needed to assess the environmental impact derived from Tl presence and to design effective remediation protocols.

ACKNOWLEDGEMENTS

This work was supported by the Spanish Ministry of Economy and Competitiveness under the research project CTM2014-55321. MA. Gomez-Gonzalez was supported by the Ph.D. fellowship program FPI (BES-2011-046461). ICP-OES/MS analyses were performed at *Servicio de análisis químico (Servicio General de Apoyo a la*

Investigación-SAI), Universidad de Zaragoza. We are grateful to Marta Furio, Alberto Jorge, Cristina Paradella, Laura Tormo and Rafael Gonzalez for their assistance in the ESEM-CL and X-Ray Diffraction analyses performed at the Museo Nacional de Ciencias Naturales (CSIC, Madrid) facilities.

LIST OF FIGURES

Figure 1 – Topographic map of Community of Madrid, with the experimental locations studied: Guadalix, S1 and Bustarviejo, S2 (a). 'Mónica mine' snapshot (Bustarviejo, site S2) and relative distances between sampling points (b). 'El Verdugal area' snapshot (Guadalix, site S1) and relative distances between sampling points (c).

Figure 2 – Section of natural Tl hosting minerals in rocks from the waste piles of S1 (a) and in-detail area of study with their relative mineral phases (b) (note that the experimental plot in 2a is not shown in size scale). ESEM-EDS (c) and cathodoluminescence (CL) (d) analyses are also presented.

Figure 3 – Section of natural Tl hosting minerals in rocks from the waste piles of S2 with their relative mineral phases (a). Backscattering (b) and monochromatic CL analyses (c) of the studied area. ESEM-EDS quantification (d) and CL spectra of K- and Na-feldspar (e) are also shown.

Figure 4 – Examples of Tl-hosting minerals (a and b) and silicon-organic phases (e and f) in S1 downstream samples, combined ESEM-EDS (c) and CL (d) analyses

Figure 5 – Examples of Tl-hosting minerals (a and b) and silicon-organic phases (e and f) in S2 downstream samples, combined ESEM-EDS (c) and CL (d) analyses

REFERENCES

Barnishel R, Bertsch PM. Methods of Soil Analysis. Part 2. Chemical, Microbiological Properties. Aluminium 1982; American Society of Agronomy: 275-300.

BOCM. Orden 2720/2006, 11 de agosto. 2007; 204: 29-30.

Council-Directive. 92/43/EEC of 21 May 1992 on the conservation of natural habitats and of wild fauna and flora (OJ 1992 L 206, pp. 7-50).

Gee GW, Bauder JW. Methods of Soil Analyses. Part 1. Physical and mineralogical methods 1986; Particle-size analyses. Madison, WI.: 383-411.

Gelabert A, Pokrovsky OS, Schott J, Boudou A, Feurtet-Mazel A, Mielczarski J, et al. Study of diatoms/aqueous solution interface. I. Acid-base equilibria and

spectroscopic observation of freshwater and marine species. Geochimica Et Cosmochimica Acta 2004; 68: 4039-4058.

Gelabert A, Pokrovsky OS, Viers J, Schott J, Boudou A, Feurtet-Mazel A. Interaction between zinc and freshwater and marine diatom species: Surface complexation and Zn isotope fractionation. Geochimica Et Cosmochimica Acta 2006; 70: 839-857.

Gomez-Gonzalez MA, Garcia-Guinea J, Garrido F, Townsend PD, Marco JF. Thallium and manganese complexes involved in the luminescence emission of potassium-bearing aluminosilicates. Journal of Luminescence 2015; 159: 197-206.

Gomez-Gonzalez MA, Serrano S, Laborda F, Garrido F. Spread and partitioning of arsenic in soils from a mine waste site in Madrid province (Spain). Science of the Total Environment 2014; 500–501: 23-33.

Gonzalez-Davila M, Santana-Casiano JM, Laglera LM. Copper adsorption in diatom cultures. Marine Chemistry 2000; 70: 161-170.

Helmhart M, O'Day PA, Garcia-Guinea J, Serrano S, Garrido F. Arsenic, Copper, and Zinc Leaching through Preferential Flow in Mining-Impacted Soils. Soil Science Society of America Journal 2012; 76: 449-462.

Ikramuddin M, Asmeron Y, Nordstrom PM, Kinart KP, Martin WM, Digby SJM, et al. Thallium: A potential guide to mineral-deposits. Journal of Geochemical Exploration 1983; 19: 465-490.

Jacobson AR, McBride MB, Baveye P, Steenhuis TS. Environmental factors determining the trace-level sorption of silver and thallium to soils. Science of the Total Environment 2005; 345: 191-205.

Jakubowska M, Pasieczna A, Zembrzuski W, Swit Z, Lukaszewski Z. Thallium in fractions of soil formed on floodplain terraces. Chemosphere 2007; 66: 611-618.

Karbowska B, Zembrzuski, W, Jakubowska M, Wojtkowiak T, Pasieczna A, Lukaszewski Z. Translocation and mobility of thallium from zinc-lead ores. Journal of Geochemical Exploration 2014; 143: 127-135.

Lis J, Pasieczna A, Karbowska B, Zembrzuski W, Lukaszewski Z. Thallium in soils and stream sediments of a Zn-Pb mining and smelting area. Environmental Science & Technology 2003; 37: 4569-4572.

Lopez Anton MA, Spears DA, Diaz Somoano M, Martinez Tarazona MR. Thallium in coal: Analysis and environmental implications. Fuel 2013; 105: 13-18.

Martin-Crespo T, Vindel E, Lopez-Garcia JA, Cardellach E. As-(Ag) sulphide veins in the Spanish Central System: further evidence for a hydrothermal event of Permian age. Ore Geology Reviews 2004; 25: 199-219.

Martin F, Garcia I, Dorronsoro C, Simon M, Aguilar J, Ortiz I, et al. Thallium behavior in soils polluted by pyrite tailings (Aznalcollar, Spain). Soil & Sediment Contamination 2004; 13: 25-36.

Martinez-Sanchez MJ, Perez-Sirvent C, Garcia-Lorenzo ML, Tudela ML, Molina J, Bech J. Background and baseline values for thallium and antimony in soils from Murcia Region (SE, Spain) and their relationship with mineralogical composition. Geophyscial Research Abstracts 2009; 11.

Massa PJ, Ikramuddin M. Thallium in gold-silver-bearing quartz veins and associated volcanic-rocks from the Como mining district, Nevada, USA. Chemical Geology 1986; 54: 27-34.

Moreno-Jimenez E, Manzano R, Esteban E, Penalosa J. The fate of arsenic in soils adjacent to an old mine site (Bustarviejo, Spain): mobility and transfer to native flora. Journal of Soils and Sediments 2010; 10: 301-312.

Moreno-Jimenez E, Penalosa JM, Manzano R, Carpena-Ruiz RO, Gamarra R, Esteban E. Heavy metals distribution in soils surrounding an abandoned mine in NW Madrid (Spain) and their transference to wild flora. Journal of Hazardous Materials 2009; 162: 854-859.

Peacock CL, Moon EM. Oxidative scavenging of thallium by birnessite: Explanation for thallium enrichment and stable isotope fractionation in marine ferromanganese precipitates. Geochimica et Cosmochimica Acta 2012; 84: 297-313.

Peter ALJ, Viraraghavan T. Thallium: a review of public health and environmental concerns. Environment International 2005; 31: 493-501.

Pokrovsky OS, Gelabert A, Viers J, Schott J, Boudou A, Feurtet-Mazel A. Study of diatoms/aqueous solution interface. II. Interaction of trace metals (Zn, Cu, Cd, Pb, Cr, Al) with freshwater and marine diatoms. Geochimica Et Cosmochimica Acta 2002; 66: A609-A609.

Rauret G, Lopez-Sanchez JF, Sahuquillo A, Rubio R, Davidson C, Ure A, et al. Improvement of the BCR three step sequential extraction procedure prior to the certification of new sediment and soil reference materials. Journal of Environmental Monitoring 1999; 1: 57-61.

Recio-Vazquez L, Garcia-Guinea J, Carral P, Maria Alvarez A, Garrido F. Arsenic mining waste in the catchment area of the Madrid Detrital Aquifer (Spain). Water Air and Soil Pollution 2011; 214: 307-320.

Scheckel KG, Lombi E, Rock SA, McLaughlin MJ. In vivo synchrotron study of thallium speciation and compartmentation in lberis intermedia. Environmental Science & Technology 2004; 38: 5095-5100.

Shah MT, Ikramuddin M, Shervais JW. Behaviour of Tl relative to K, Rb, Sr. Ba in mineralized and unmineralized metavolcanics from the Dir area, northern Pakistan. Mineralium Deposita 1994; 29: 422-426.

Smeaton CM, Walshe GE, Fryer BJ, Weisener CG. Reductive Dissolution of Tl(I)–Jarosite by Shewanella putrefaciens: Providing New Insights into Tl Biogeochemistry. Environmental Science & Technology 2012; 46: 11086-11094.

Stafilov T, Sajn R, Alijagic J. Distribution of Arsenic, Antimony, and Thallium in Soil in Kavadarci and its Surroundings, Republic of Macedonia. Soil & Sediment Contamination 2013; 22: 105-118.

Tatsi K, Turner A. Distributions and concentrations of thallium in surface waters of a region impacted by historical metal mining (Cornwall, UK). Science of the Total Environment 2014; 473: 139-146.

Thomas GW. Methods of Soil Analysis, Part 2. Chemical and Microbiological Properties. Exchangeable cations 1982; Soil Science Society of America: 159-166.

Tremel A, Masson P, Sterckeman T, Baize D, Mench M. Thallium in French agrosystems .1. Thallium contents in arable soils. Environmental Pollution 1997; 95: 293-302.

Vanek A, Chrastny V, Komarek M, Penizek V, Teper L, Cabala J, et al. Geochemical position of thallium in soils from a smelter-impacted area. Journal of Geochemical Exploration 2013; 124: 176-182.

Vanek A, Groesslova Z, Mihaljevic M, Ettler V, Chrastny V, Komarek M, et al. Thallium contamination of soils/vegetation as affected by sphalerite weathering: A model rhizospheric experiment. Journal of Hazardous Materials 2015; 283: 148-156.

Vanek A, Komarek M, Vokurkova P, Mihaljevic M, Sebek O, Panuskova G, et al. Effect of illite and birnessite on thallium retention and bioavailability in contaminated soils. Journal of Hazardous Materials 2011; 191: 170-176.

Villar M, Alava F, Lavilla I, Bendicho C. Operational speciation of thallium in environmental solid samples by electrothermal atomic absorption spectrometry according to the BCR sequential extraction scheme. Journal of Analytical Atomic Spectrometry 2001; 16: 1424-1428.

Walkley A, Black IA. An examination of the Degtjareff method for determining soil organic matter, and a proposed modification of the chromic acid titration method. Soil Science 1934; 37: 29-38.

Xiao T, Yang F, Li S, Zheng B, Ning Z. Thallium pollution in China: A geo-environmental perspective. Science of the Total Environment 2012; 421: 51-58.

Xiao TF, Guha J, Boyle D, Liu CQ, Zheng BS, Wilson GC, et al. Naturally occurring thallium: a hidden geoenvironmental health hazard? Environment International 2004; 30: 501-507.

Yang C, Chen Y, Peng P, Li C, Chang X, Xie C. Distribution of natural and anthropogenic thallium in the soils in an industrial pyrite slag disposing area. Science of the Total Environment 2005; 341: 159-172.

Zitko V. Toxicity and pollution potential of thallium. The Science of the total environment 1975; 4: 185-92.

Table 1 – Sequential extraction steps for thallium fractionation [a]

Step	Phase desired	Extraction conditions
FI	Exchangeable, carbonates and hydroxides	20 mL HOAc (0.11 M, pH 2.8), 25 ºC, 16 h, continual agitation
FII	Fe/Mn oxide-hydroxides	20 mL $NH_2OH \cdot HCl$ (0.5 M, pH 1.5), 25 ºC, 16 h, continual agitation
FIII	Organic matter or sulfides	5 mL H_2O_2 (30%), 85 ºC, 1 h, intermittent agitation; 25 mL NH_3OAc (1.0 M, pH 2.0), 25 ºC, 16 h, continual agitation
R	Aluminosilicates and other crystallized minerals	HCl:HNO_3:HF (ratio 3.5:0.75:1.5), H_3BO_3 (5%), microwave-assisted digestion

[a] Procedure based on Yang et al.(2005). Initial sample weight = 0.5 g

Table 2 – Physical and chemical properties of the bulk samples

Sample	pH	EC[a]	Ca^{2+}	Mg^{2+}	Na^{+}	K^{+}	Al^{3+}	ECEC[b]	TOC[c]	Sand	Silt	Clay
		$\mu S\ cm^{-1}$	$cmol_c\ kg^{-1}$						%	%		
S1-WP	3.3	2330	78.8	0.04	0.04	0.04	0.08	79.0	0.03	53	-	47
S1-RB	4.6	87.6	0.69	0.30	0.72	0.21	0.88	2.81	0.17	71	16	12
S1-SP	6.1	110	3.19	1.05	0.22	0.18	0.21	4.84	0.20	70	18	12
S1-F	6.4	105	1.56	0.45	0.10	0.06	0.81	2.99	0.54	88	3.6	8
S2-WP	3.5	137	0.63	0.26	0.18	0.13	1.11	2.31	0.21	84	9	7
S2-A	6.6	30.8	28.6	11.2	0.68	1.11	0.04	41.7	1.47	76	16	8
S2-B	6.7	54.8	26.6	10.4	0.69	1.17	0.01	38.9	4.73	79	16	5
S2-C	6.5	22.3	8.96	3.00	0.23	0.23	0.01	12.4	5.46	49	40	11

[a] Electrical conductivity
[b] Effective Cation Exchange Capacity as calculated from the sum of exchangeable cations
[c] Total Organic Carbon determined by wet digestion (Walkley and Black, 1934)

Table 3 – Main mineral phases of soil samples (< 2 mm) as determined by XRD analyses

Sample	*Major phases*				*Minor phases*	
S1-WP	Scorodite	Gypsum			Hematite	
S1-RB	Illite	Kaolinite	Quartz		Muscovite	
S1-SP	Illite	Microcline	Kaolinite	Albite	Quartz	Montmorillonite
S1-F	Illite	Albite	Microcline	Quartz	Kaolinite	
S2-WP	Quartz	Microcline	Illite	Albite	Kaolinite	Jarosite
S2-A	Quartz	Albite	Microcline		Illite	Orthoclase
S2-B	Albite	Quartz	Illite		Microcline	Kaolinite
S2-C	Albite	Quartz			Illite	Microcline

Table 4 – Element concentration of soil samples

Sample	As [a]	CV [b]	Mn [a]	CV [b]	Pb [a]	CV [b]	Fe [c]	CV [b]	Tl [a]	CV
	mg kg^{-1}	%	mg kg^{-1}	%	mg kg^{-1}	%	mg kg^{-1}	%	mg kg^{-1}	%
S1-WP	143900	0.005	1599	0.9	507	1.1	252300	0.2	2.65	9.3
S1-RB	6220	0.1	357	7.2	- [e]	- [e]	45530	1.0	1.54	10.7
S1-SP	94.4	1.0	265	8.8	30.3	11.7	16980	1.8	1.34	3.1
S1-F	60.4	3.1	376	6.3	30.6	8.3	16330	1.7	1.30	0.8
S2-WP	28210	0.03	148	9.7	3428	0.2	59680	0.9	2.19	0.9
S2-A	4063	0.2	1513	8.6	524	1.3	33100	1.2	1.26	2.7
S2-B	2458	1.3	2032	1.8	286	1.8	20590	2.0	0.87	9.8
S2-C	1334	0.3	1242	8.0	306	2.7	27660	1.3	0.94	10.7
CRM	80	7.1	687	11.5	1160	16.7	26190	1.1	2.54	8.4
CRM values[e]	105 ± 8		638 ± 28		1162 ± 31		28900 ± 600		2.47 ± 0.15	

[a] As, Mn, Pb and Tl concentrations were measured by ICP-MS after microwave-assisted digestion
[b] Coefficient of variation (CV) defined as the standard deviation (n=3) divided by the mean value which represents the instrumental variability of the ICP measurements
[c] Fe concentration was measured by ICP-OES after microwave-assisted digestion
[d] Below detection limit
[e] Reference certified concentrations values and estimated relative standard deviations of SRM 2711 Montana soil as certified by the National Institute of Standards and Technology (NIST)

Table 5 – Solid phase distribution of thallium determined by the BCR sequential extraction procedure [a]

Sample	**FI**			**FII**			**FIII**			**R**			Sum I-R[e]	Total[f]
	m [b]	sd [c]	% [d]	m	sd	%	m	sd	%	m	sd	%	mg·kg^{-1}	mg·kg^{-1}
S1-WP	0.05	0.00	1.69	0.17	0.01	6.09	0.09	0.00	3.13	2.43	0.22	89.1	2.72	2.65
S1-RB	0.00	0.00	0.07	0.04	0.00	3.62	0.04	0.00	3.61	1.21	0.13	93.5	1.30	1.54
S1-SP	0.00	0.00	0.08	0.01	0.00	1.09	0.01	0.00	0.90	1.07	0.07	97.9	1.09	1.34
S1-F	0.00	0.00	0.08	0.02	0.00	1.70	0.01	0.00	1.35	1.09	0.03	97.1	1.13	1.30
S2-WP	0.00	0.00	0.05	0.10	0.01	5.40	0.02	0.00	1.00	1.73	0.09	93.8	1.84	2.19
S2-A	0.01	0.00	1.02	0.09	0.01	7.94	0.03	0.00	2.32	1.06	0.04	88.7	1.19	1.26
S2-B	0.03	0.00	3.22	0.09	0.01	11.3	0.02	0.00	2.42	0.67	0.09	83.7	0.80	0.87
S2-C	0.00	0.00	0.11	0.04	0.00	4.86	0.03	0.00	3.64	0.78	0.08	91.4	0.86	0.94
CRM	0.06	0.00	2.37	0.45	0.02	18.4	0.21	0.00	8.58	1.73	0.06	70.6	2.46	2.54

[a] The BCR procedure is described in Table 1
[b] Mean value of extracted Tl in the corresponding BCR step calculated by ICP-MS, in mg·kg^{-1}
[c] Standard deviation of three replicate BCR steps, in mg·kg^{-1}
[d] Percentage of extracted Tl respect to the sum of the BCR steps (I-II-III-R)
[e] Extracted Tl as the sum of the BCR steps (I-II-III-R)
[f] Total concentration of Tl in samples measured by ICP-MS (Table 4)

Figure 1

Click here to download high resolution image

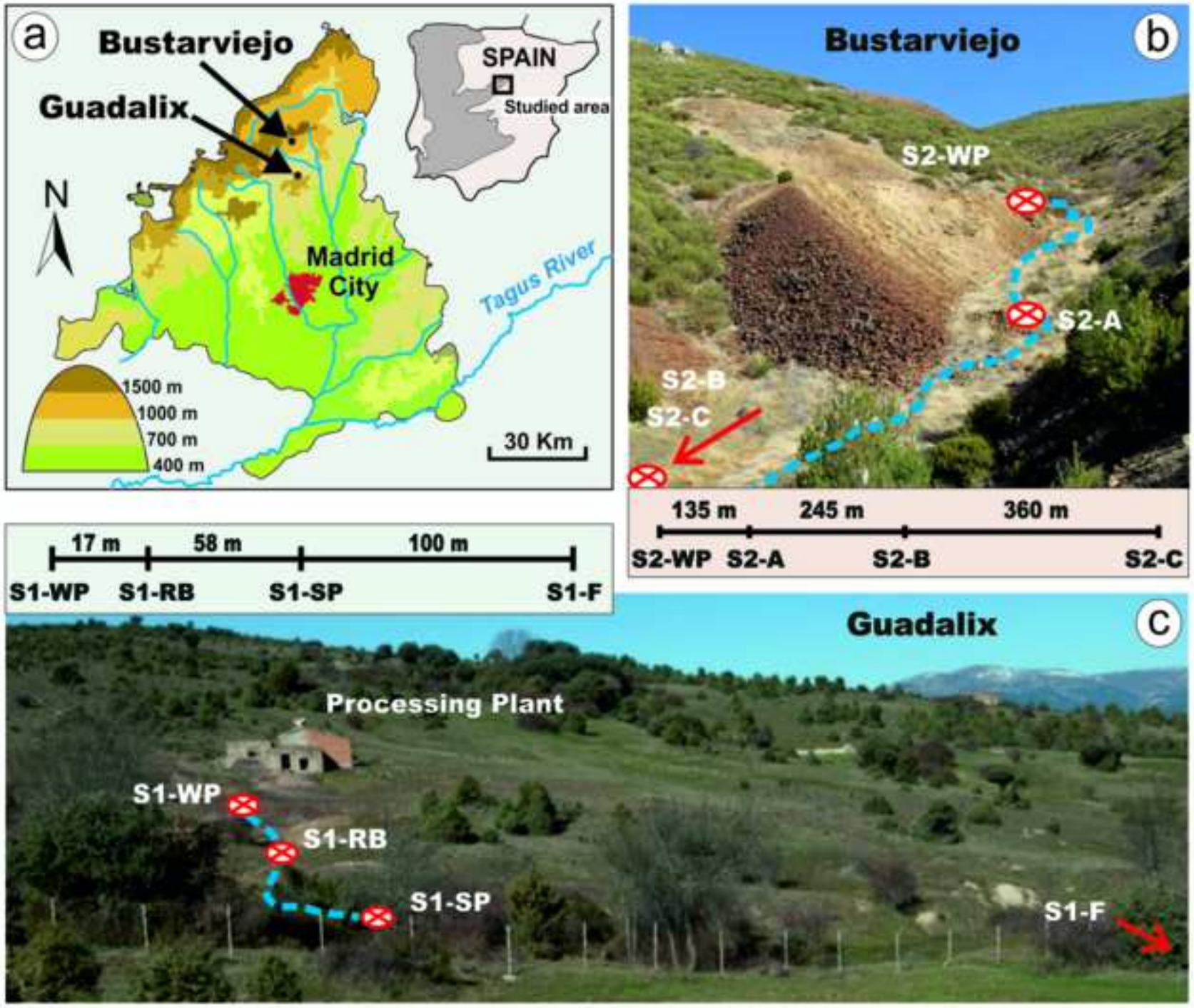

Figure 2

Click here to download high resolution image

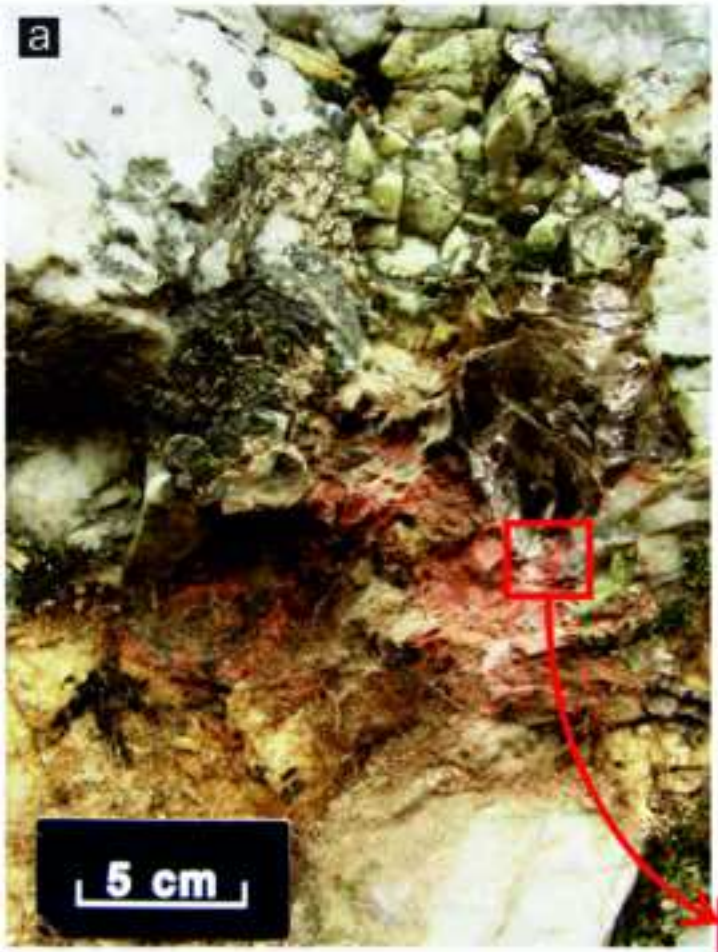

c

	① K-Feld	② K-Feld	③ Na-Feld	④ Quartz	⑤ Mosc	⑥ Monaz	⑦ Mn-Nod	⑧ Baryte
Al K	7.1	7.8	8.5	0.2	17.6			
Si K	20.2	24.4	24.1	41.9	23.7			
P K	0.6					12.6	2.7	
S K								14.6
As L							0.8	
Ca K			0.1				0.4	
Na K	0.4	0.2	8.0		0.4			
K K	7.4	9.1	0.1		8.9			
Mn K					0.1		45.2	
Fe K	16.6		0.3	0.7	3.1		7.9	
Cu K							1.0	
Ba L								56.9
Pb M							19.8	
Ag L						0.9		
La L						15.3		
Ce L						23.7		
Nd L						6.0		
Tl M	0.3	0.5	0.4	0.8	0.2			0.1
O	47.4	58.0	58.5	56.4	46.0	41.5	22.2	28.4
Total	100	100	100	100	100	100	100	100

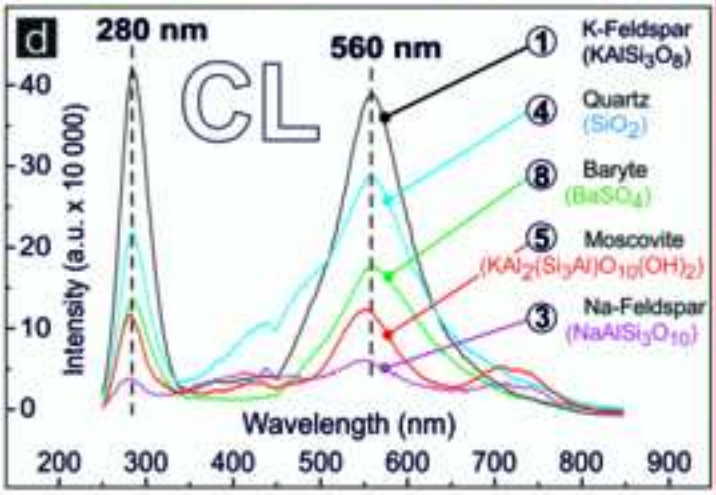

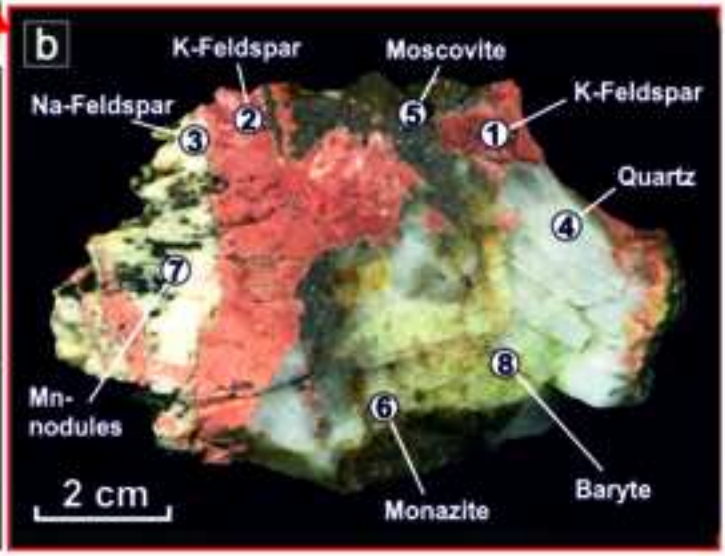

Figure 3

Click here to download high resolution image

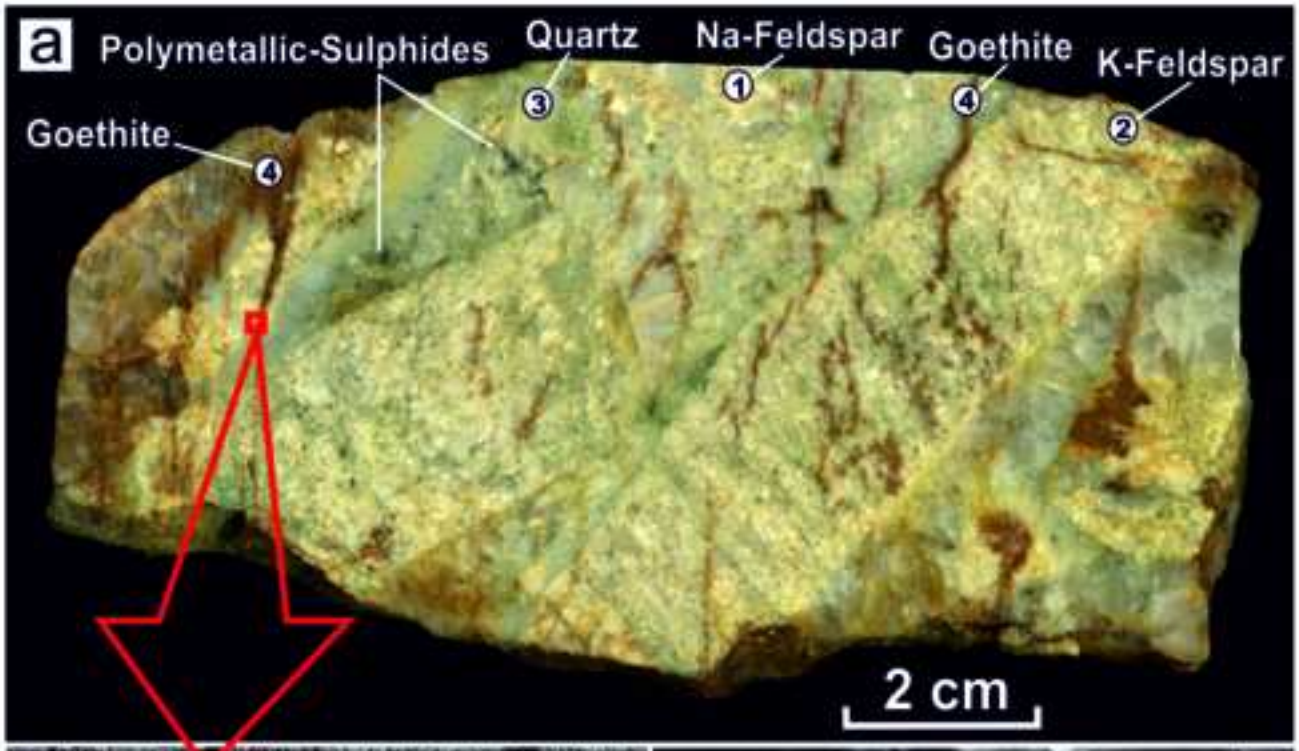

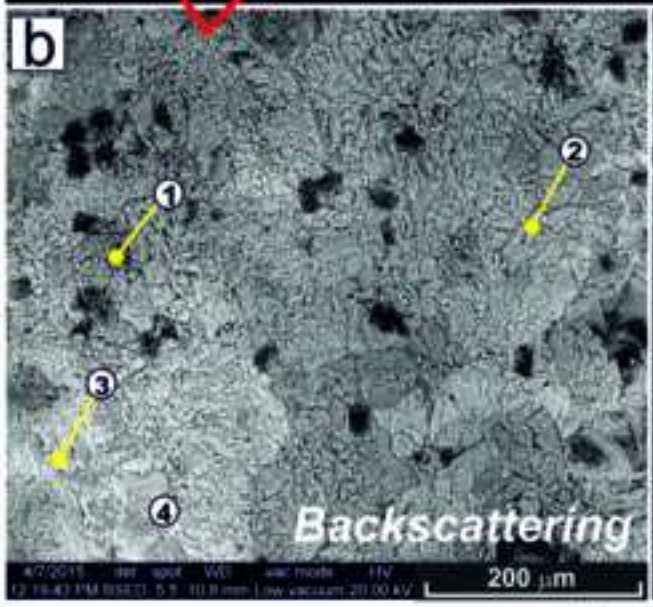

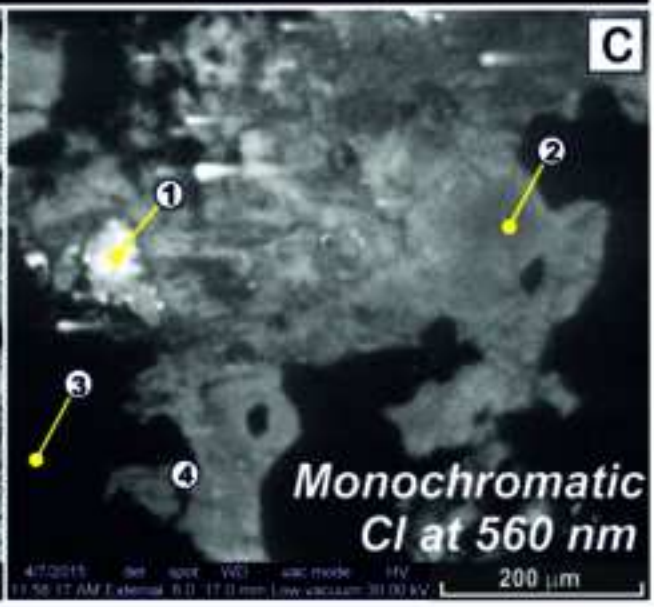

d

	① Na-Feld	② K-Feld	③ Quartz	④ Goethite
Na K	7.4	1.0		
Al K	9.5	9.5	0.4	0.6
Si K	32.4	30.7	44.4	0.9
S K			0.9	0.9
K K	1.4	11.2		
Ca K	0.2			
Fe K		0.9	1.4	66.2
Cu K				
Sn L				
Tl M	0.7	0.3		
O	48.4	46.4	52.9	31.4
Total	100	100	100	100

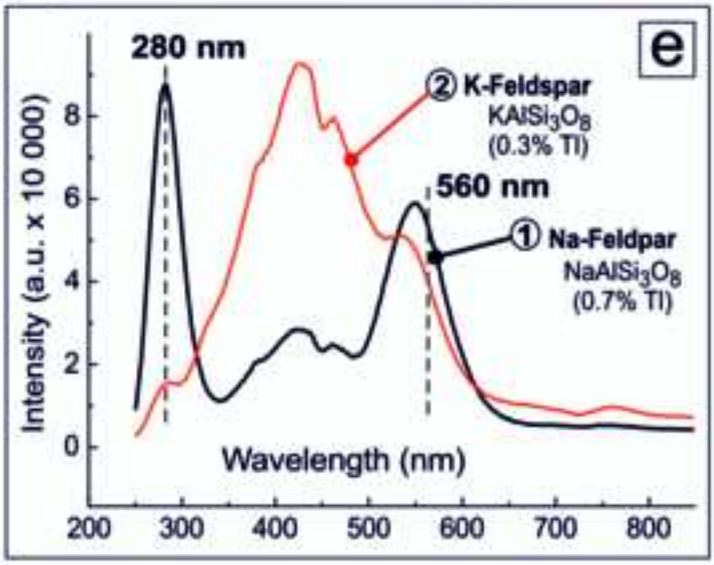

Figure 4

Click here to download high resolution image

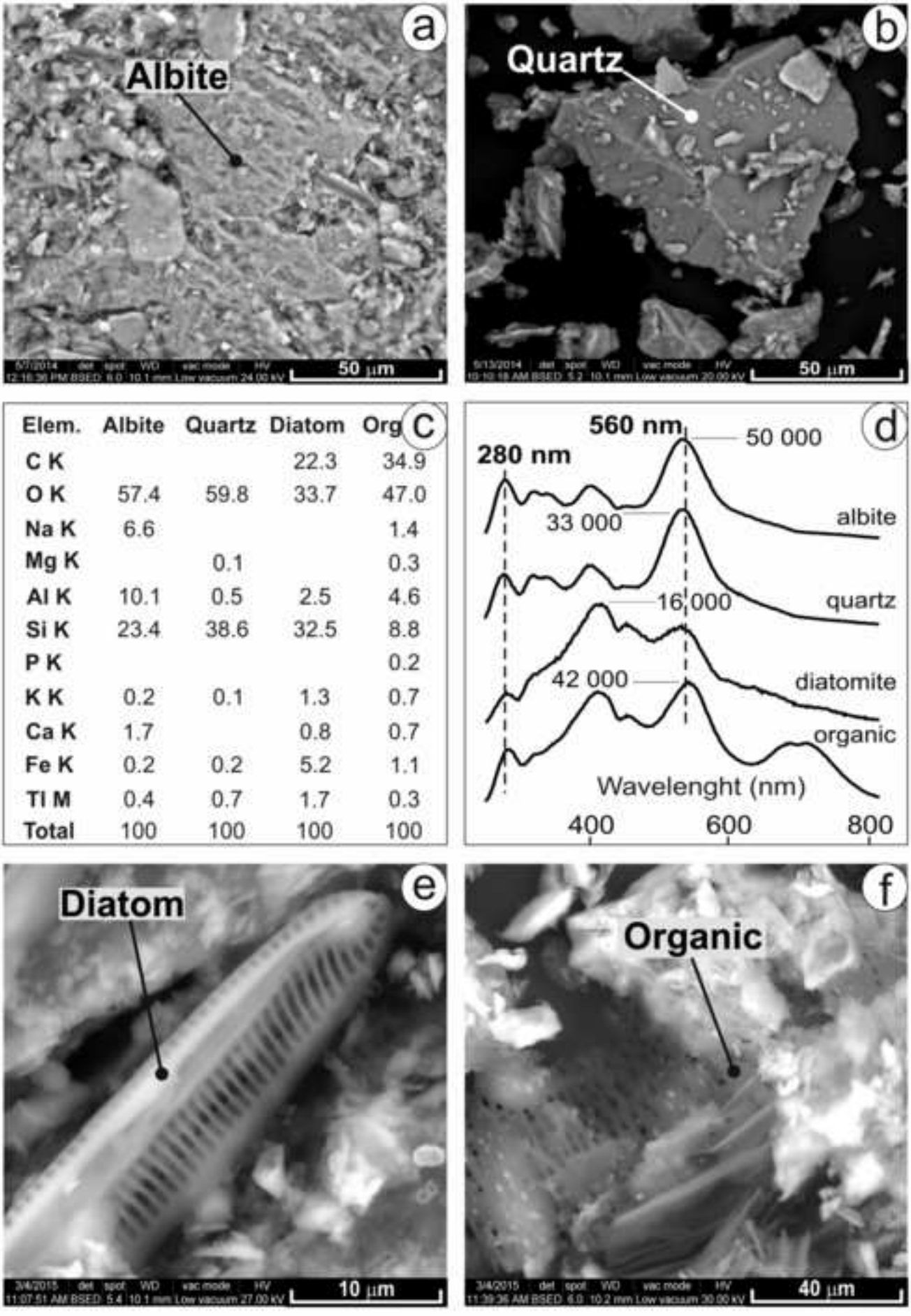

Elem.	Albite	Quartz	Diatom	Org
C K			22.3	34.9
O K	57.4	59.8	33.7	47.0
Na K	6.6			1.4
Mg K		0.1		0.3
Al K	10.1	0.5	2.5	4.6
Si K	23.4	38.6	32.5	8.8
P K				0.2
K K	0.2	0.1	1.3	0.7
Ca K	1.7		0.8	0.7
Fe K	0.2	0.2	5.2	1.1
Tl M	0.4	0.7	1.7	0.3
Total	100	100	100	100

Figure 5

Click here to download high resolution image

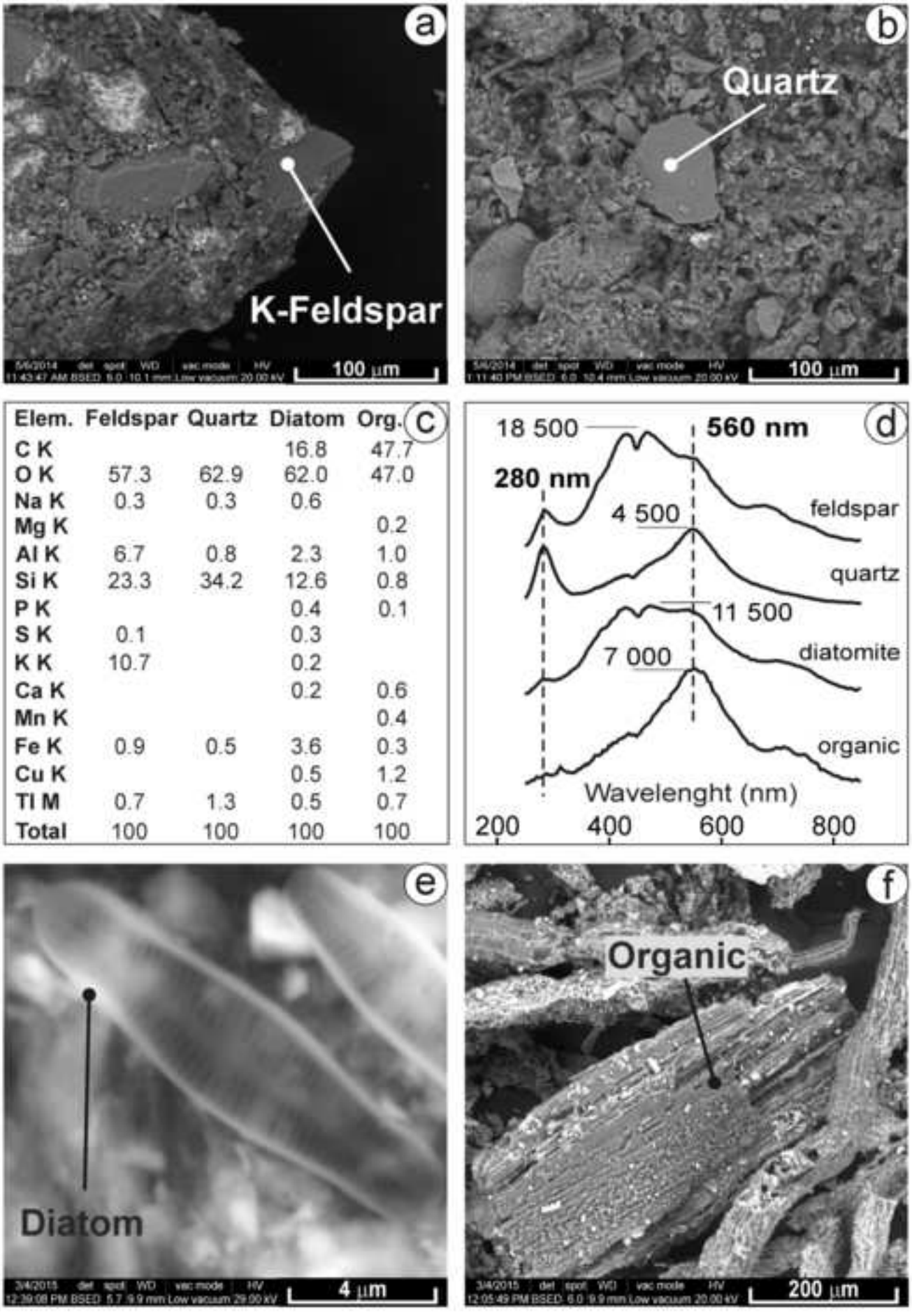

Elem.	Feldspar	Quartz	Diatom	Org.
C K			16.8	47.7
O K	57.3	62.9	62.0	47.0
Na K	0.3	0.3	0.6	
Mg K				0.2
Al K	6.7	0.8	2.3	1.0
Si K	23.3	34.2	12.6	0.8
P K			0.4	0.1
S K	0.1		0.3	
K K	10.7		0.2	
Ca K			0.2	0.6
Mn K				0.4
Fe K	0.9	0.5	3.6	0.3
Cu K			0.5	1.2
Tl M	0.7	1.3	0.5	0.7
Total	100	100	100	100